



Research article

Ajith P. Ravishankar*, Marvin A.J. van Tilburg^a, Felix Vennberg, Dennis Visser and Srinivasan Anand*

Color generation from self-organized metallo-dielectric nanopillar arrays

<https://doi.org/10.1515/nanoph-2019-0171>

Received June 10, 2019; revised July 19, 2019; accepted July 23, 2019

Abstract: Nanostructures composed of dielectric, metallic or metallo-dielectric structures are receiving significant attention due to their unique capabilities to manipulate light for a wide range of functions such as spectral colors, anti-reflection and enhanced light-matter interaction. The optical properties of such nanostructures are determined not only by the shape and dimensions of the structures but also by their spatial arrangement. Here, we demonstrate the generation of vivid colors from nanostructures composed of spatially disordered metallo-dielectric (In/InP) nanopillar arrays. The nanopillars are formed by a single-step, ion-sputtering-assisted, self-assembly process that is inherently scalable and avoids complex patterning and deposition procedures. The In/InP nanopillar dimensions can be changed in a controlled manner by varying the sputter duration, resulting in reflective colors from pale blue to dark red. The fast Fourier transform (FFT) analysis of the distribution of the formed nanopillars shows that they are spatially disordered. The electromagnetic simulations combined with the optical measurements show that the reflectance spectra are strongly influenced by the pillar dimensions. While the specular and diffuse reflectance components are appreciable in all the nanopillar samples, the specular part dominates for the shorter nanopillars, thereby leading to a glossy effect. The simulation results show that the characteristic features in the observed specular and diffused reflectance spectra are determined by the modal and light-scattering properties of single pillars.

While the work focuses on the In/InP system, the findings are relevant in a wider context of structural color generation from other types of metallo-dielectric nanopillar arrays.

Keywords: structural colors; InP; disorder; reflectance; waveguide modes.

1 Introduction

Structural colors are ubiquitous in nature. These are observed in a wide variety of living organisms, for example, from the wings of Morpho species of butterflies, the scales of *Lamprocyphus augustus* weevil beetles or peacock feathers [1–4]. Unlike dyes, where colors are produced by the selective absorption and emission of light by the dye molecules, the structural colors are manifestations of different forms of behavior of light in micro- and nano-structured materials and depend on the geometry of the structures and their spatial arrangements. The optical phenomena contributing to the structural colors can be resonant scattering, structure and material dependent absorption, diffraction or multilayer thin-film interference [1, 5, 6]. Dyes and pigments are vulnerable to photo bleaching and they can degrade over time. In this regard, structural colors are advantageous as their optical properties are mostly governed by the physical and material parameters of the structured media [4–8]. Research on the structural colors both in reflection and transmission has led to a stream of potential real-life applications that include high-density printing [9, 10], color filters [11], sensors [12], biomimetic devices [13, 14], artificial camouflage [15] and colored solar cells [16, 17]. Precise control over the way by which the incident light interacts with nanostructures is necessary to obtain the desired spectral characteristics over the entire visible wavelength range. This can be achieved through specific choices of the material properties (e.g. refractive index, absorption) and geometrical designs for the nanostructures (e.g. dimensions, shape and spatial arrangement). One of the simplest ways

*Present address: Department of Applied Physics, Eindhoven University of Technology, 5600 MB Eindhoven, Netherlands

*Corresponding authors: Ajith P. Ravishankar and Srinivasan Anand: Department of Applied Physics, KTH Royal Institute of Technology, Electrum 229, S-164 40 Kista, Sweden, e-mail: aprav@kth.se (A.P. Ravishankar); anand@kth.se (S. Anand). <https://orcid.org/0000-0003-3333-9492> (A.P. Ravishankar)

Marvin A.J. van Tilburg, Felix Vennberg and Dennis Visser: Department of Applied Physics, KTH Royal Institute of Technology, Electrum 229, S-164 40 Kista, Sweden

to achieve colors is by exploiting the optical interference at the interfaces of multilayer or ultra-thin films [5, 18]. Nanostructures on both high and low index dielectric substrates also exhibit a wide range of colors through wavelength-dependent light scattering and/or coupling to resonant modes. For example, semiconductor nanopillar/nanodisk arrays display reflective colors that are mainly determined by the resonant modes in the structure and, in some cases, together with the material absorption [19–23]. Color filters have been fabricated by randomly texturing polymers with wavelength-dependent light-scattering properties that depend on the topography of the texture [24]. Vibrant colors have also been achieved using metallic nanostructures, such as nanodisks and gratings, by enhancing localized plasmon resonances [25–28].

Most of the cases mentioned above are nanostructures designed for the visible wavelength regime, and the structures and their spatial separations are in the few tens to few hundreds of nanometers. Achieving precision in the fabrication of these optical nanostructures is important as the optical properties are sensitive to the shapes and spatial distributions of the nanostructures. Top-down methods (nanopatterning and etching), bottom-up methods (self-assembly and solution synthesis) or their combinations have been used extensively to achieve the desired nanostructures. E-beam lithography (EBL) is most commonly used for patterning small areas due to its flexibility and high precision. Alternative methods for low-cost and large area nanopatterning, such as imprinting or colloidal lithography, are also used, but these often involve multi-step procedures [29–32]. The ion-sputtering-assisted formation of self-organized nanostructures, as reported in this work, is an interesting phenomenon that can be used to fabricate disordered nanopillar arrays (DNPA) in a single-step wafer scale process. With this procedure, it is possible to obtain uniform color all over the wafer without additional processing steps, such as pattern generation, metal deposition and subsequent etching.

The ion bombardment of III-V surfaces, such as InP and GaSb, results in the formation of self-organized nanopillars on the surface [33–36]. The preferential sputtering of the group V species leads to excess group III species (here, Ga or In) on the surface, which diffuse and coalesce to form self-assembled nano-islands. These (metallic) nano-islands function as self-generated etch masks for nanopillar formation, resulting in metallo-dielectric DNPA. In addition, the spatial arrangement of the metal-capped nanopillars can be disordered, thereby reducing coherent scattering. Unlike other topics, such metallo-dielectric nanopillar arrays with spatial disorder have received much less research attention in the context of

structural color generation. However, the fabrication of hybrid Au(Cr)-Si metallo-dielectric nanostructures has been reported, and the results demonstrate unique optical properties by re-shaping the metal nanodisk on top of a Si nanocone [37]. The high refractive index contrast between the nanostructures and the surrounding ambient/matrix is advantageous in tuning the optical properties. High-index nanostructures can efficiently confine electromagnetic fields and support different kinds of resonant modes depending on their dimensions. Therefore, tuning the shapes and sizes of individual structures can lead to sharp changes in the reflection features [19–21]. The III-V semiconductor materials are promising candidates in this regard as most of these materials have refractive indices above 3 in the visible wavelength region. Even though there have been ample studies on silicon-based color generation [19, 38–40], very few attempts have been made in the context of III-V materials, which are important for several optoelectronic applications, such as photodetectors and solar cells [21, 41, 42].

In this work, we report on the generation of reflective colors from metallo-dielectric (In/InP) DNPA. The In/InP nanopillars are fabricated by a thermally driven, ion-sputtering-assisted, self-assembly process. We demonstrate that it is possible to generate, in a simple one-step process, spatially disordered nanopillars with sub-wavelength dimensions and average spacings. Vivid colors are obtained by tuning the nanopillar dimensions. By detailed optical measurements and electromagnetic simulations, we investigate the structural color generation from In/InP nanopillars, including the role of their dimensions and spatial arrangements. The spectral characteristics of the specular and diffused reflectance are separately investigated to identify the modal and scattering contributions to each of these components. We analyze the size-dependent absorption in the InP nanopillars and demonstrate how it plays an important role in determining the dips in the specular reflectance. The light-scattering properties of individual nanopillars are also examined in detail to explain the spectral characteristics of the diffused reflectance.

2 Experimental methods

To generate the In/InP nanopillars, the InP substrates (typically 1 cm² in size) at 270°C were sputtered using 400 eV nitrogen ion beam. Sputtering times varied between 30 s to 4 min, which increased the nanopillar height and diameter from ~240–650 nm and ~140–220 nm, respectively. For these nanopillar dimensions, a range of vivid colors as shown in Figure 1A were obtained.

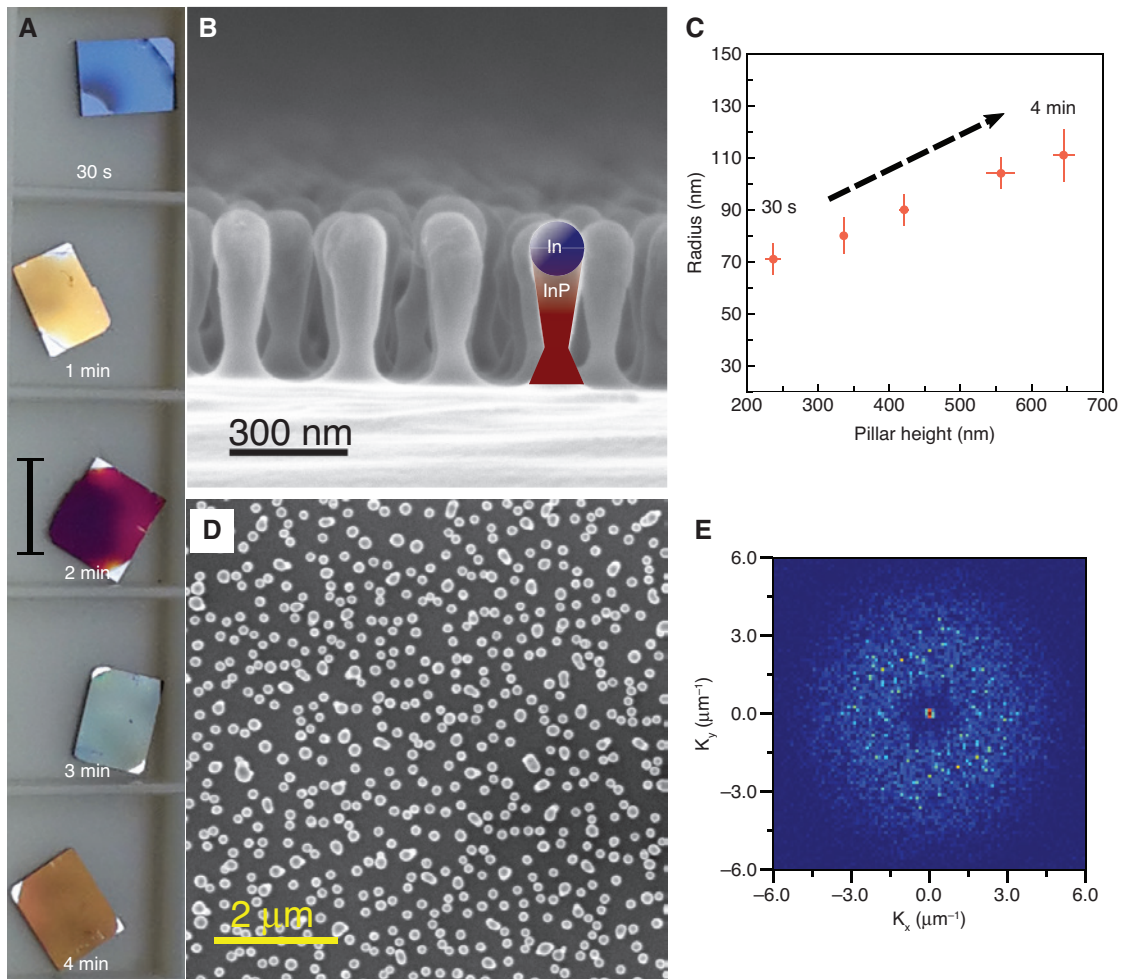


Figure 1: Morphology and spatial distribution of DNPA.

(A) The camera images showing the reflective colors from different In/InP DNPA fabricated by ion sputtering for different time durations. The scale bar on the 2 min sample image corresponds to 1 cm. (B) Representative cross-sectional scanning electron microscope (SEM) image of the In/InP nanopillars. The inset shows a simple schematic of the formed nanopillar with In-rich capping. (C) Relations between the nanopillar radii (as measured from top-view SEM) and their heights. (D) Representative top view SEM image of the In/InP nanopillars suggesting a disordered spatial arrangement. (E) The FFT of the SEM image in (D) is isotropic, demonstrating the disordered spatial arrangement of the nanopillars; the spatial frequencies span the visible wavelength region.

The physical mechanism of the nanopillar formation and the process details are discussed in detail in Ref. [34]. A representative cross-sectional scanning electron micrograph (SEM) showing the dimensions and shapes of the nanopillars formed by 2 min sputtering is shown in Figure 1B. From our previous studies, detailed material analysis reveals that these nanopillars contain an In-rich ball-like cap on top of the InP pillars [34]. This is shown schematically in the inset of Figure 1B. As can be seen, all nanopillar samples have similar properties, albeit different in their dimensions. The relations between the nanopillar radii (i.e. of the In-rich cap) obtained from the top view SEM images and their heights for different sputter times are plotted in Figure 1C. With increasing sputter times, their heights increase along with the average radii of the

In-cap due to continued buildup of In during the process. Within a given sample, the heights and radii of the pillars show small variations (Figure 1C). However, a few coalesced pillars could also be found (Figure 1D). The spatial arrangement of the nanopillars appears disordered. The 2D fast Fourier transform (FFT) of the image is shown in Figure 1E. The isotropic distribution of spatial frequencies and the lack of discrete peaks in FFT image clearly show that the nanopillars are spatially disordered, thereby implying that coherent scattering is unlikely. In all the nanopillar samples, the estimated average nearest neighbor distances (~250–320 nm) are in subwavelength range (Supplementary material, Table S1).

Reflectance spectra from the nanopillar assembly were measured using Perkin Elmer Lambda 950 UV/Vis/NIR

spectrophotometer. The total reflectance was obtained by restricting the reflected light within an integrating sphere, and the diffused reflectance was measured from the light remaining inside integrating sphere after directing the specular light out. The specular reflectance was then calculated by subtracting the diffused from the total reflectance. The total reflectance measured for samples with different nanopillar heights (Figure 2A) clearly shows distinct reflectance spectra corresponding to the observed colors (Figure 1A). For larger pillar heights (>420 nm), the total reflectance is reduced in the entire spectral region. Interestingly, the colors disappear in all the samples when the top portions of the pillars (amorphous InP and the In-cap) are removed using a hydrogen fluoride (HF)

treatment. The representative results are shown in the Supplementary material, Figure S2, where one can note the associated featureless reflectance spectrum. These observations indicate the importance of the dimensions, shape and material composition of the In/InP nanopillars in generating colors.

3 Results and discussion

To gain insights into the origin of spectral colors, we simulated the optical properties of the In/InP nanopillars by the finite difference time domain (FDTD) method using the Lumerical commercial software [43]. As discussed

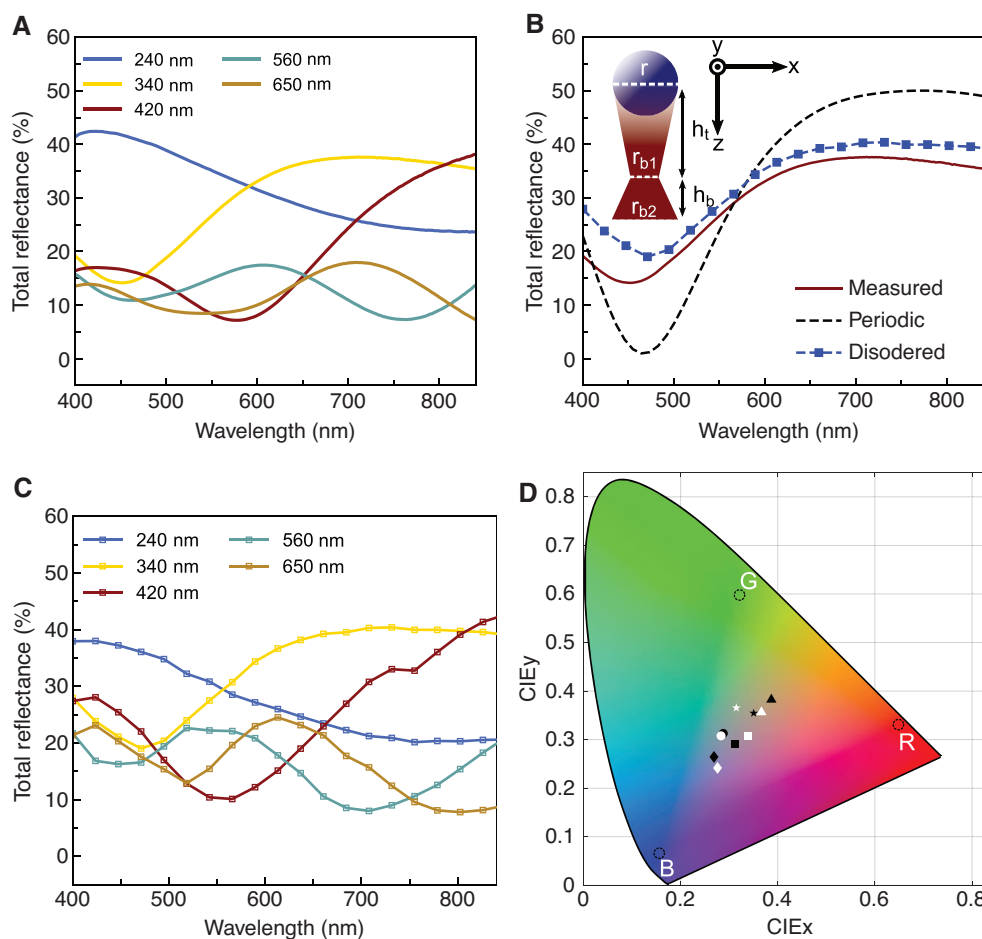


Figure 2: Total reflectance and color characteristics of DNPA.

(A) The experimentally measured total reflectance from self-assembled In/InP DNPA samples of different average heights. (B) Comparison of the experimental and simulated total reflectance from pillars with the height of ~340 nm demonstrates the influence of the ordered (periodic) and disordered (supercell) arrangement of pillars. Inset: Schematic of the metallo-dielectric pillar model incorporating the tapered profile of the InP pillar and In sphere at the top of the pillar. This pillar model was adopted in all of the FDTD simulations. (C) The total reflectance results from the FDTD simulations with supercell approximation on the nanopillar assemblies of different heights. (D) Representation of the measured (white) and simulated (black) reflectance colors on CIE 1931 color map. The markers – circle, triangle, diamond, star and square – are the chromaticity values for the reflective colors from the nanopillar assemblies with heights of 240 nm, 340 nm, 420 nm, 560 nm and 650 nm respectively.

previously, material analysis on self-assembled In/InP nanopillars has shown In-rich capping on top of the InP pillars composed of amorphous and crystalline regions [34]. Accordingly, we modelled the material composition of the In/InP pillars. To keep the model simple, we approximate the In-rich capping as a sphere and the InP part to be composed of amorphous InP (a-InP). The shape parameters (r , h_t , h_b , r_{b1} and r_{b2}) are illustrated in the inset of Figure 2B. The quantitative details of the shape parameters and the nearest neighbor distances are provided in the supplementary information section (Supplementary material, Table S1). As a simple simulation setup, we arranged pillars in a square lattice. The average nearest neighbor distance and the average In-cap radius, as determined by the top-view SEM images, were used for the period and the In sphere radius (r), respectively. A plane polarized light source (400–850 nm) was incident normally in the z direction. Total reflectance was calculated from a field monitor placed behind the source. The refractive indices for the In and InP substrates were taken from Palik [44] and that for the a-InP substrate came from the Adachi database [45]. Perfectly matched layers (PML) were used on the z boundaries and periodic boundary conditions (BC) on the x and y boundaries. Figure 2B shows the simulated reflectance data for an In/InP nanopillar (height: 340 nm; In-cap radius: 80 nm) square array (period: 280 nm). Although the reflectance dip and peak positions are in qualitative agreement with the experimental data, the intensities show significant deviations. Changing the period from 250 to 400 nm does not have a dramatic effect on the position of the reflectance dip, while the overall reflectance is influenced to a certain extent (Supplementary material, Figure S3). However, changing the pillar shape and material composition does play a major role in determining the reflectance spectra (Supplementary material, Figure S4).

In order to obtain accurate reflectance spectra from the simulations, variations in the diameters and the heights of the pillars along with their disordered arrangement have to be considered. Therefore, we adopted a supercell approximation to be able to use periodic BC in the simulations without losing the disordered nature of pillar arrangement. We took the supercell of $\sim 6 \mu\text{m}^2$ for this purpose. Within this boundary, the pillars are positioned at coordinates extracted from the top view SEM images along with their respective In-cap radii (r). For this supercell, periodic BCs were used on the x and y boundaries and PML on the z boundaries. The above approach closely represents the disorder in the nanopillar assembly. As shown in Figure 2A–C, the reflectance data obtained from these simulations are in quantitative

agreement with the measured spectra for all the samples. As the simulations of the disordered nanopillar assemblies are computationally intensive, as discussed earlier (Figure 2B), it might still be useful to consider periodic arrangements in predicting the qualitative trends, such as reflectance dips and peak positions. Figure 2D shows the chromaticity positions on the CIE 1931 color map of the reflective colors (measured and simulated) from the In/InP nanopillar assemblies with different pillar heights. The details of the x , y chromaticity parameter calculations are provided in the Supplementary material. Though the colors reside within the standard RGB range, they are not as extended in the color gamut as presented in recent studies [22, 25]. The chromaticity values estimated from the simulated and the measured reflectance spectra are in reasonable agreement.

It is important to determine the extent to which the diffuse and specular components contribute to the reflected color. For example, the color and glossiness can vary depending on the spectral intensities of the specular and diffuse reflectances [5]. Therefore, it is necessary to study them individually and understand their physical origins. As seen on Figure 3A and B, the diffused and specular reflectances dominate in different spectral ranges, except for the short pillars for which the latter is consistently higher in the full visible range. For shorter pillars (height < 420 nm) measurements show that the specular part dominates (Figure 3A) over the diffused part (Figure 3B) resulting in a glossy appearance. Although the diffused reflectance has different spectral characteristics depending on the nanopillar height, the intensity variation is within $\sim 5\%$ – 15% . From the simulated total reflectance (Figure 2D), the specular component was calculated by extracting only the zeroth grating order from the field monitors and the diffused component by summing over the rest of the orders. These results, together with the measured data, are shown in Figure 3A and B. The similarity in the simulated and experimental spectra strongly supports the considered physical model for the nanopillars and the approximations used in the simulations to model the spatial disorder of the nanopillars.

It is interesting to analyze the role of a spatially disordered nanopillar arrangement on the specular and the diffused reflectance. To address this issue, one approach is to introduce spatial randomness to a periodically arranged nanopillar system [46]. The disorder was obtained by displacing individual pillars in a square lattice to a new position (P^{rand}) by a constant distance from their original positions (P^0); however, the direction in which they are displaced is random. Quantitatively,

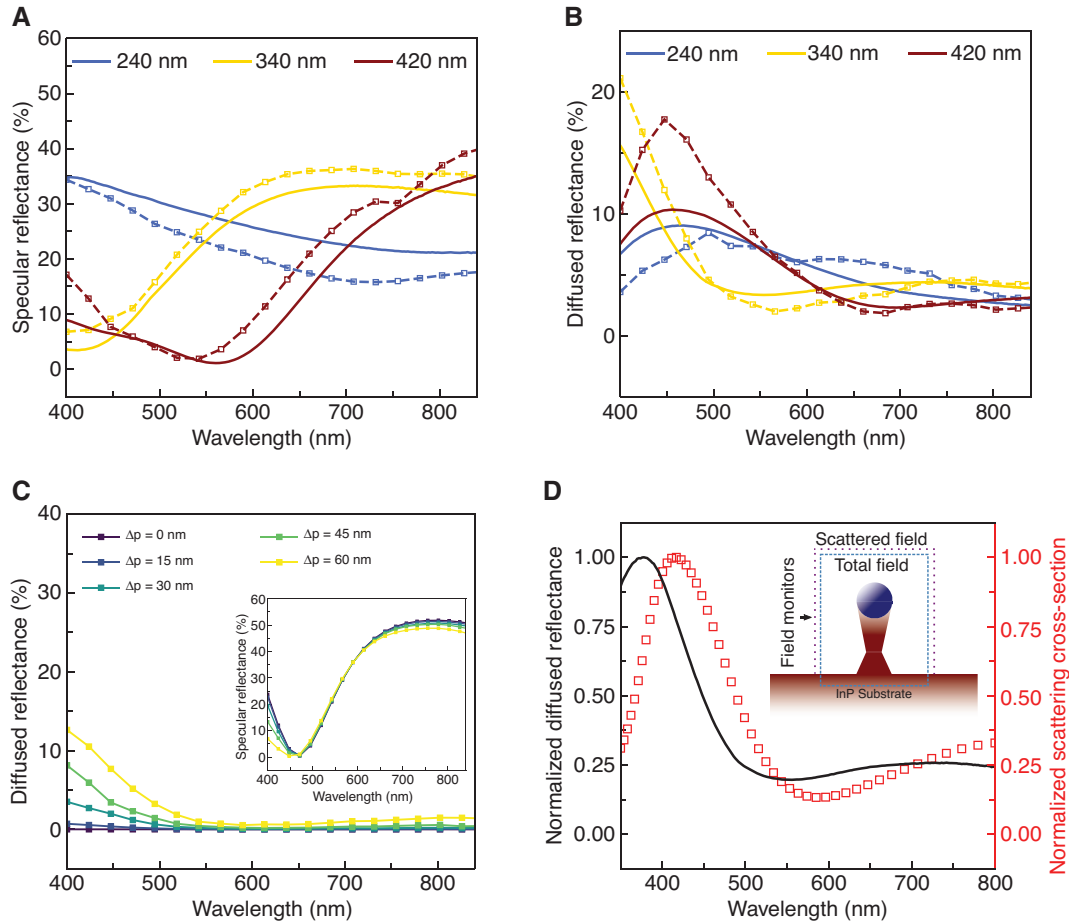


Figure 3: Specular and diffused spectral characteristics of DNPAs.

The comparison of (A) the specular and (B) the diffused reflectances obtained from the measurements (solid lines) and FDTD simulations (dashed lines) of the fabricated DNPA with different nanopillar heights. (C) The simulated diffused reflectances for different extents of spatial disorder (Δp) in the nanopillar arrangement; the pillar height is 340 nm. Inset: The change in the specular component. (D) The normalized diffused reflectance (measured) for a DNPA sample and scattering cross-section (simulated) of a single pillar. The pillar height is 340 nm. Inset: The scattering cross-section was calculated using field monitors (dashed line) placed outside the TFSF source (solid line) and above the InP substrate.

this can be represented in Cartesian coordinates as $P_x^{\text{rand}} = P_x^o + \Delta p \cos \theta^{\text{rand}}$ and $P_y^{\text{rand}} = P_y^o + \Delta p \sin \theta^{\text{rand}}$, where Δp is the amount of displacement in the position of pillars and θ^{rand} is a random value between 0 to 2π . With this definition, Δp is a measure of disorder. Given that only the center-center distance is taken into account and not the lateral size of the pillars, there is a possibility that pillars overlap with increasing Δp . To avoid this, we limited the pillar displacement Δp to ~ 60 nm for pillars with a diameter of 160 nm. Using the nanopillar spatial coordinates as determined by the above procedure, we simulated the reflectance using supercell approximations. The results are shown in Figure 3C. By increasing Δp , from 0 (periodic) to 60 nm, the diffused reflectance at shorter wavelengths (~ 400 – 500 nm) increased by up to $\sim 12\%$ and a corresponding reduction in the specular reflectance can be observed (Figure 3C inset).

The above observations clearly suggest that the diffused reflectance increases with the disorder and can be attributed to the scattering from individual pillars. To establish this, we investigated light scattering from a single nanopillar on the InP substrate. The simulations were performed using a total field scattered field (TFSF) source incident normally in the z direction. The results are shown in Figure 3D. The inset shows the schematic of the simulation set-up. The scattering cross-section was calculated using field monitors (X, Y and Z normal) placed outside the TFSF source. The Z-normal monitor was placed only above the pillar. This ensured that only the scattered light not coupled to the substrate was collected. Scattering cross-section (σ) was estimated for each monitor by normalizing the transmission power measured by each of the monitors with the source intensity. The total scattering cross-section was obtained by summing the cross-section values

obtained from all the monitors. As shown in Figure 3D, the measured diffused spectrum closely matched the normalized scattering cross-section of the individual pillars. Similar results were obtained for other nanopillar heights (Supplementary material, Figure S5). Thus, the diffused reflectance from the DNPA is primarily determined by the scattering properties of individual pillars. Moreover, the analysis on field intensity profiles of pillars within TFSF boundary (Supplementary material, Figure S6) shows that field intensity maxima occur near the In cap for wavelength close to peak wavelength in the diffused reflectance spectrum. We attribute the diffused reflectance peak to the scattering resonances associated with the In sphere on top of the high-index dielectric nanopillar. Furthermore, simulations comparing the In/InP and InP (both having the same shape) show that the In/InP model (Figure 2B) is in excellent agreement with the measurements (Supplementary material, Figure S5).

The scattering cross-section peaks match well with the peaks in the diffused spectra (Figure 3B, Figure S4). Importantly, the peaks in the diffused reflectance (Figure 3B) do not overlap with the reflection dips observed in the total (Figure 2A) and in the specular (Figure 3A) reflectance spectra. We also performed the TFSF simulations (considering a non-absorbing substrate but with the same refractive index as InP) to determine the scattering into the substrate. Here, the scattering cross-section peak again occurs at the spectral peak position of the diffused reflectance. Considering the above, we believe that the spectral dip (Figures 2A and 3A) must have originated from a different resonant phenomena. The specular reflectance level (Figure 3A) is also clearly higher than the diffused reflectance level (Figure 3B). In the total reflectance (Figure 2A) from the pillars with heights of ~340 or 420 nm, the spectral dip position observed in both the specular and total reflectance has greater influence on the overall coloration. In the metallo-dielectric nanopillars, such phenomena as size-dependent resonant coupling (including absorption) in the dielectric and/or plasmonic nanostructures can be expected to influence the reflectance characteristics. For the metallic nanostructures, the reflectance dips may correspond to the excitation of localized surface plasmon resonances (LSPR) for specific structural dimensions [25, 27]. Although the self-organized pillars have metal (In)-rich capping, the plasmonic resonances of In fall in the ultraviolet wavelength region [47, 48]. Thus, for the In/InP DNPA, the direct plasmonic origin for the specular structural colors is unlikely. The observed specular reflectance characteristics are likely due to the size-dependent resonant absorption in the semiconductor nanopillars [19, 21, 41]. As the pillar height increases, their diameters

also increase from 140 to 220 nm (Figure 1C). As shown in Figure 3A, no clear reflectance dips/peaks are observed for the shortest pillars, whereas a clear dip is seen for the other samples. Pillars taller than 500 nm invariably show more than one reflectance dip (Supplementary material, Figure S7). Studies on silicon vertical nanopillars have shown that hybrid modes (HE_{11}) can be excited and, consequently, the resonant absorption can occur at specific wavelengths depending on pillar diameter [49]. For wider pillars, the resonant absorption also occurs due to the higher order modes and the absorption peak can also broaden for the tapered/conical pillars [49, 50]. Therefore, we expect such modal properties to be present even in the case of the In/InP DNPA.

To verify the role of the nanopillar size in the resonant absorption, an analysis was performed to investigate the absorption in the In/InP nanopillars. Power absorption in a material depends both on electric field intensity $|E|^2$ and the absorption co-efficient of the material at a given frequency (ω). The total power dissipation in a material within a given volume of V can be evaluated as $\int_V 0.5\omega\epsilon''|E|^2 dV$, where ϵ'' is the imaginary part of the permittivity of the material. Using Lumerical, the power absorption analysis was performed for pillars in a square lattice with periodic BCs. This choice is reasonable as the spectral position of the specular reflectance dip is not sensitive to the arrangement of the nanopillars. Figure 4A and B show a clear relationship between peaks in the total absorption spectra and the dip positions in the specular reflectance spectra. Further, the absorption peak red shifts with the increasing height and diameter of the nanopillars. When the refractive index contrast between the resonator and the substrate is low, the light couples more into the substrate making the resonance weaker. The coupling of resonant modes into the substrate can be avoided by separating the resonator using a pedestal narrow enough to decouple the structure from the substrate [51]. In our case, the neck at the base of the InP nanopillars are not narrow enough compared with the rest of the pillar above (Figure 1B) and hence the pillars are not optically isolated (de-coupled) from the substrate. The InP is a direct bandgap semiconductor ($E_g \sim 1.34$ eV) and efficiently absorbs the above band gap light within 1–2 μm . The absorption of the guided light in the pillars depends on the wavelength and the height of the fabricated nanopillars. To estimate the amount of light transmitted into the substrate, we simulated the reflectance and transmittance of the In/InP nanopillars on a non-absorbing substrate but having the same refractive index of bulk InP. The absorption (A) is then calculated as 1-R-T, where R is the reflectance and T is the transmittance of light into the substrate. The results presented in the Supplementary material,

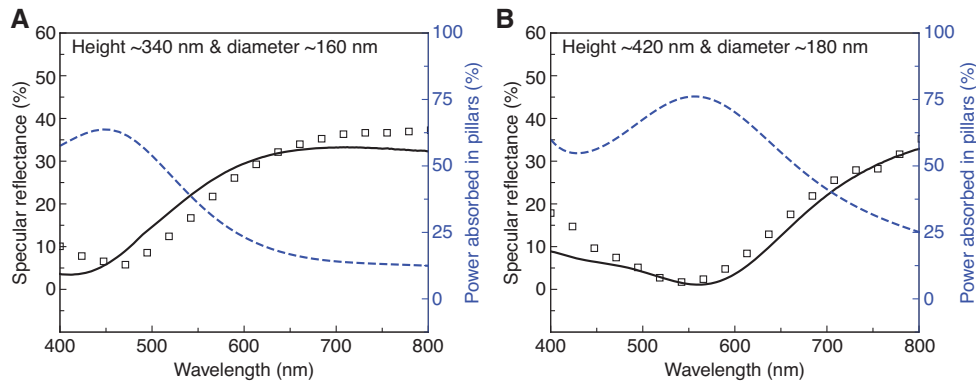


Figure 4: Relation between absorption spectral peak of an In/InP nanopillar and specular reflectance dip of DNPAs.

The comparison between the specular spectral features (solid black lines are measured and square markers are simulated using supercell approximations) and power absorbed in the pillars (blue dashed lines obtained from periodic array simulations) for pillar diameters (A) ~ 160 nm and (B) ~ 180 nm. The results show that the specular spectral dips occur very close to the pillar absorption peaks.

Figure S7 show that part of the light is transmitted to the substrate and part of it is absorbed within the pillars. Importantly, the absorption values calculated using this approach are clearly maximized near the reflectance dips and are comparable with the results obtained using the poynting vector approach (Figure 4). From the cross-section profile of power absorption in a pillar with a height

of 340 nm (Figure 5A), we observe that higher absorption occurs closer to the metal dielectric interface due to field enhancement. In comparison, the cross-sectional electric field intensity profile (Figure 5B) of the nanopillar at the resonant wavelength shows that the HE_{1m} like modes are supported within the pillar. Therefore, it is evident that the dips in the specular reflectance originate from the coupling

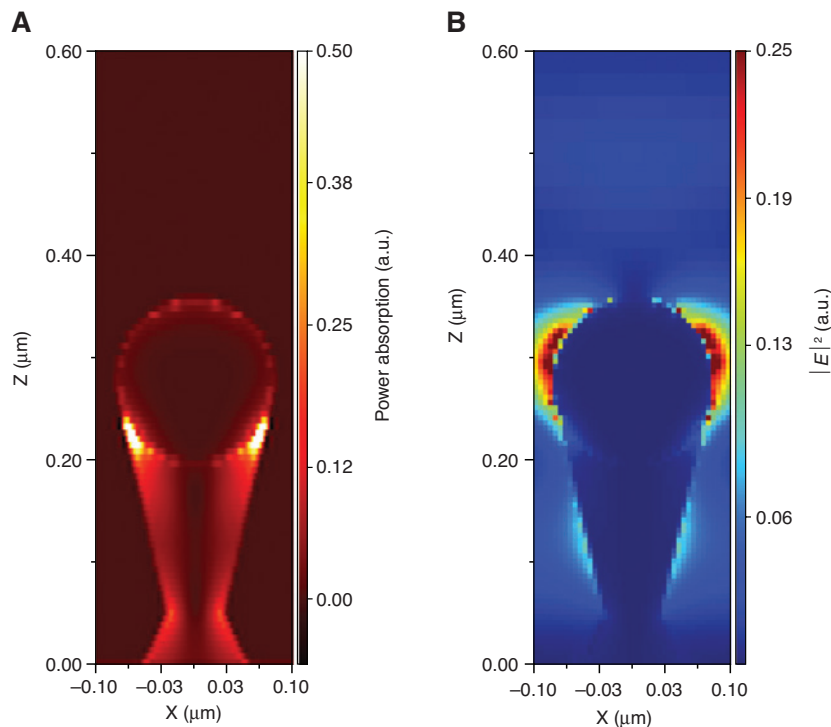


Figure 5: Power absorption and electric field intensity profiles of an In/InP nanopillar.

The cross-section profile of (A) power absorption and (B) electric field intensity ($|E|^2$) for a pillar with a height of ~ 340 nm at an incident light wavelength of 445 nm clearly show absorption within the pillars and presence of a HE_{1m} -like mode in the tapered InP nanopillar. Both the profiles have been normalized to the maximum value of the respective parameters. To enhance the profile within the pillars, the parameter values were saturated to 0.5 for the power absorption profile and 0.25 for the electric field intensity profile.

of light to the pillar waveguide modes (HE_{lm} like) and from the subsequent absorption of the light within the pillar. As the pillars have conical geometry with diameters changing from 160 nm at the top to 60 nm at the bottom neck of the pillar, it is difficult to describe the exact mode supported in the pillars. A quantitative comparison between the total absorption and the specular intensity can also meet difficulties in evaluating such disordered distribution of pillars. To deduce the exact relations among them, the waveguide resonance/scattering studies must be conducted directly on the ensemble of pillars. However, analysis on the ordered pillars are still beneficial in predicting the spectral behaviors of specular and diffused components. By exploring the fabrication methods that can tune the physical aspects of the individual pillars, the color features of the total reflectance can be controlled and optimized.

4 Conclusions

We have demonstrated structural colors in reflection from metallo-dielectric (In/InP) DNPA. We realized the DNPA array on the InP substrates using the ion beam sputtering method. With this method, wafer scale uniform color from the In/InP DNPA can be obtained in a single step, as opposed to using wafer scale patterning, metal deposition and subsequent etching. However, to realize the macro-scaled color variations in a given wafer, a multi-step fabrication procedure, which might include masking steps, is necessary. The fabricated nanopillars have In-rich capping on top of the InP nanopillars. The FFT analysis shows that the arrangement of the nanopillars is subwavelength and disordered. The reflective colors from pale blue to dark red can be generated from the DNPA by varying only the sputter duration and within a small range from 30 s to 4 min. The optical measurements show that both specular and diffused reflectance contribute to the color generation. A higher specular contribution in the pillars of smaller heights (<420 nm) leads to glossy colors from these samples. The FDTD simulations on the In/InP pillar model, with supercell approximations on the arrangement of pillars, matches well with the experimentally observed reflectance spectra. Though simulations with supercell approximations is a better approach, simulations using periodic boundary conditions can also be considered to estimate qualitative spectral features in the reflectance profile. By introducing spatial disorder to the periodic arrangement of pillars, we observe that diffused reflectance increases with increasing disorder. Scattering studies using the TFSF simulations show that the spectral peaks in the diffused reflectance

are related to the scattering cross-section of the individual pillars. In comparison, the spectral features in the specular reflectance originate from the modal (HE_{lm} -like) coupling of light into the pillars and its absorption within these pillars. Overall, the studies on the In/InP DNPA show that the color features can be characterized by describing the interactions of light with an individual pillar. By controlling the shape and the size of individual pillars, we can effectively tune the spectral behavior of the diffused and the specular components of the total reflectance.

Furthermore, the analysis can be extended to other types of metallo-dielectric DNPA from which spectral colors are expected. Our future studies will focus on improving the range of colors by optimizing the process parameters for pillar formation and by appropriately selecting the refractive indices of the substrate and the surrounding medium. For example, the In/InP DNPA can be fabricated from InP thin films provided on a low-index substrate instead of using the InP substrates. Similarly, the nanopillars can be embedded in a low-index (e.g. 1.5) transparent medium.

Supplementary material

Included in the supplementary material are the details regarding dimensions of the nanopillars considered for the simulations (Table S1), the effect of removing the top portion of the nanopillars on the colors (Figure S1), relevant FDTD simulation results (Figures S2–S7) and the chromaticity calculations for the reflective colors.

Acknowledgments: The authors acknowledge Yohan Désières for useful discussions.

Funding sources: The funding for this work came from the Swedish Research Council (Vetenskapsrådet; Grant Nos.: 349-2007-8664, Funder Id: <http://dx.doi.org/10.13039/501100004359> and 621-2014-5078, Funder Id: <http://dx.doi.org/10.13039/501100004359>) and the Swedish Energy Agency (Energimyndigheten; grant: 45199-1, Funder Id: <http://dx.doi.org/10.13039/501100004527>).

References

- [1] Vukusic P, Sambles JR. Photonic structures in biology. *Nature* 2003;424:852.
- [2] Yoshioka S, Kinoshita S. Wavelength-selective and anisotropic light-diffusing scale on the wing of the Morpho butterfly. *Proc R Soc Lond B Biol* 2004;271:581–7.

- [3] Galusha JW, Richey LR, Gardner JS, Cha JN, Bartl MH. Discovery of a diamond-based photonic crystal structure in beetle scales. *Phys Rev E* 2008;77:050904.
- [4] Zi J, Yu X, Li Y, et al. Coloration strategies in peacock feathers. *Proc Natl Acad Sci* 2003;100:12576–8.
- [5] Kinoshita S, Yoshioka S, Miyazaki J. Physics of structural colors. *Rep Prog Phys* 2008;71:076401.
- [6] Prum RO, Torres RH, Williamson S, Dyck J. Coherent light scattering by blue feather barb. *Nature* 1998;396:28.
- [7] Park JG, Kim SH, Magkiriadou S, Choi TM, Kim YS, Manoharan VN. Full-spectrum photonic pigments with non-iridescent structural colors through colloidal assembly. *Angew Chem Int Edit* 2014;53:2899–903.
- [8] Sun J, Bhushan B, Tong J. Structural coloration in nature. *RSC Adv* 2013;3:14862–89.
- [9] Zhu X, Yan W, Levy U, Mortensen NA, Kristensen A. Resonant laser printing of structural colors on high-index dielectric metasurfaces. *Sci Adv* 2017;3:1602487.
- [10] Kumar K, Duan H, Hegde RS, Koh SC, Wei JN, Yang JK. Printing colour at the optical diffraction limit. *Nat Nanotechnol* 2012;7:557.
- [11] Park CS, Shrestha VR, Yue W, et al. Structural color filters enabled by a dielectric metasurface incorporating hydrogenated amorphous silicon nanodisks. *Sci Rep* 2017;7:2556.
- [12] Lee JH, Fan B, Samdin TD, et al. Phage-based structural color sensors and their pattern recognition sensing system. *ACS Nano* 2017;11:3632–41.
- [13] Parker AR, Townley HE. Biomimetics of photonic nanostructures. *Nat Nanotechnol* 2007;2:347.
- [14] Kawamura A, Kohri M, Morimoto G, Nannichi Y, Taniguchi T, Kishikawa K. Full-color biomimetic photonic materials with iridescent and non-iridescent structural colors. *Sci Rep* 2016;6:33984.
- [15] Phan L, Walkup IV WG, Ordinario DD, et al. Reconfigurable infrared camouflage coatings from a cephalopod protein. *Adv Mater* 2013;25:5621–5.
- [16] Zhang W, Anaya M, Lozano G, et al. Highly efficient perovskite solar cells with tunable structural color. *Nano Lett* 2015;15:1698–702.
- [17] Neder V, Luxembourg SL, Polman A. Efficient colored silicon solar modules using integrated resonant dielectric nanoscatterers. *Appl Phys Lett* 2017;111:073902.
- [18] Kats MA, Blanchard R, Genevet P, Capasso F. Nanometre optical coatings based on strong interference effects in highly absorbing media. *Nat Mater* 2013;12:20.
- [19] Seo K, Wober M, Steinvurzel P, et al. Multicolored vertical silicon nanowires. *Nano Lett* 2011;11:1851–6.
- [20] Yang SC, Richter K, Fischer WJ. Multicolor generation using silicon nanodisk absorber. *Appl Phys Lett* 2015;106:081112.
- [21] Wu PM, Anttu N, Xu HQ, Samuelson L, Pistol ME. Colorful InAs nanowire arrays: from strong to weak absorption with geometrical tuning. *Nano Lett* 2012;12:1990–5.
- [22] Proust J, Bedu F, Gallas B, Ozerov I, Bonod N. All-dielectric colored metasurfaces with silicon Mie resonators. *ACS Nano* 2016;10:7761–7.
- [23] Sun S, Zhou Z, Zhang C, et al. All-dielectric full-color printing with TiO₂ metasurfaces. *ACS Nano* 2017;11:4445–52.
- [24] Clausen J, Christiansen AB, Garnæs J, Mortensen NA, Kristensen A. Color effects from scattering on random surface structures in dielectrics. *Opt Express* 2012;20:4376–81.
- [25] Tan SJ, Zhang L, Zhu D, et al. Plasmonic color palettes for photorealistic printing with aluminum nanostructures. *Nano Lett* 2014;14:4023–9.
- [26] Xu T, Shi H, Wu YK, Kaplan AF, Ok JG, Guo LJ. Structural colors: from plasmonic to carbon nanostructures. *Small* 2011;7:3128–36.
- [27] Roberts AS, Pors A, Albrechtsen O, Bozhevolnyi SI. Subwavelength plasmonic color printing protected for ambient use. *Nano Lett* 2014;14:783–7.
- [28] Clausen JS, Højlund-Nielsen E, Christiansen AB, et al. Plasmonic metasurfaces for coloration of plastic consumer products. *Nano Lett* 2014;14:4499–504.
- [29] Kanamori Y, Katsube H, Furuta T, Hasegawa S, Hane K. Design and fabrication of structural color filters with polymer-based guided-mode resonant gratings by nanoimprint lithography. *Jpn J Appl Phys* 2009;48:06FH04.
- [30] Liu P, Bo L, Yang J, et al. Self-assembled colloidal arrays for structural color. *Nanoscale Adv* 2019;1:1672–85.
- [31] Lee KT, Jang JY, Park SJ, et al. Angle-insensitive and CMOS-compatible subwavelength color printing. *Adv Opt Mater* 2016;4:1696–702.
- [32] Lee HS, Shim TS, Hwang H, Yang SM, Kim SH. Colloidal photonic crystals toward structural color palettes for security materials. *Chem Mater* 2013;25:2684–90.
- [33] Le Roy S, Barthel E, Brun N, Lelarge A, Søndergård E. Self-sustained etch masking: a general concept to initiate the formation of nanopatterns during ion erosion. *J Appl Phys* 2009;106:094308.
- [34] Sanatinia R, Berrier A, Dhaka V, et al. Wafer-scale self-organized InP nanopillars with controlled orientation for photovoltaic devices. *Nanotechnology* 2015;26:415304.
- [35] Murdoch BJ, Barlow AJ, Fletcher IW, Cumpson PJ. The plasmonic properties of argon cluster-bombarded InP surfaces. *Appl Phys Lett* 2017;111:081603.
- [36] Murdoch BJ, Portoles JF, Tardio S, Barlow AJ, Fletcher IW, Cumpson PJ. Visible wavelength surface-enhanced Raman spectroscopy from In-InP nanopillars for biomolecule detection. *Appl Phys Lett* 2016;109:253105.
- [37] Zuev DA, Makarov SV, Mukhin IS, et al. Fabrication of hybrid nanostructures via nanoscale laser-induced reshaping for advanced light manipulation. *Adv Mater* 2016;28:3087.
- [38] Højlund-Nielsen E, Weirich J, Nørregaard J, Garnæs J, Mortensen NA, Kristensen A. Angle-independent structural colors of silicon. *J Nanophotonics* 2014;8:083988.
- [39] Kanamori Y, Shimono M, Hane K. Fabrication of transmission color filters using silicon subwavelength gratings on quartz substrates. *IEEE Photonics Technol Lett* 2006;18:2126–8.
- [40] Flauraud V, Reyes M, Paniagua-Dominguez R, Kuznetsov AI, Brugger J. Silicon nanostructures for bright field full color prints. *ACS Photonics* 2017;4:1913–9.
- [41] Lee WJ, Senanayake P, Farrell AC, Lin A, Hung CH, Huffaker DL. High quantum efficiency nanopillar photodiodes overcoming the diffraction limit of light. *Nano Lett* 2015;16:199–204.
- [42] Wallentin J, Anttu N, Asoli D, et al. InP nanowire array solar cells achieving 13.8% efficiency by exceeding the ray optics limit. *Science* 2013;339:1057–60.
- [43] Lumerical Inc., <https://www.lumerical.com/>, (Accessed June 8, 2019).
- [44] Palik ED. Handbook of optical constants of solids. Cambridge, MA, USA, Academic Press, 1998.

- [45] Adachi S. Optical constants of crystalline and amorphous semiconductors: numerical data and graphical information. New York, USA, Springer Science & Business Media, 1999.
- [46] Kumar R, Mujumdar S. Intensity correlations in metal films with periodic-on-average random nanohole arrays. *Opt Commun* 2016;380:174–8.
- [47] Ross MB, Schatz GC. Aluminum and indium plasmonic nanoantennas in the ultraviolet. *J Phys Chem C* 2014;118:12506–14.
- [48] Kumamoto Y, Taguchi A, Honda M, Watanabe K, Saito Y, Kawata S. Indium for deep-ultraviolet surface-enhanced resonance Raman scattering. *ACS Photonics* 2014;1:598–603.
- [49] Wang B, Leu PW. Tunable and selective resonant absorption in vertical nanowires. *Opt Lett* 2012;37:3756–58.
- [50] Wang B, Leu PW. Enhanced absorption in silicon nanocone arrays for photovoltaics. *Nanotechnology* 2012;23:194003.
- [51] Garín M, Solà M, Julian A, Ortega P. Enabling silicon-on-silicon photonics with pedestalled Mie resonators. *Nanoscale* 2018;10:14406.

Supplementary Material: The online version of this article offers supplementary material (<https://doi.org/10.1515/nanoph-2019-0171>).